

Construction and Validation of a Dawn and Dusk Land Surface Temperature for MERSI-LL FY-3E (Supplementary Material)

Zhiyan Liu^{1,2}, Kazuhito Ichii^{1,2}, Yuhei Yamamoto^{1,3}, Ruci Wang¹, Hideki Kobayashi⁴, Masahito Ueyama⁵

1. Center for Environmental Remote Sensing, Chiba University, Chiba, Japan
2. Graduate School of Science and Engineering, Chiba University, Chiba, Japan
3. Institute for Advanced Academic Research, Chiba University, Chiba, Japan
4. Research Institute for Global Change, Japan Agency for Marine-Earth Science and Technology, Yokohama, Japan
5. Graduate School of Agriculture, Osaka Metropolitan University, Sakai, Japan

Contents of This File

Fig. S1. Total Precipitable Water (TPW) and simulated land surface temperature (LST) for the SeeBor profile used in this study.

Fig. S2. Atmospheric downward radiance estimated from the atmospheric upward radiance of (a) band 5, (b) band 6, and (c) band 7 of the MERSI-LL FY-3E.

Fig. S3. a) Emissivity spectra of sample materials used for training the normalized emissivity method (NEM) module. Lines represent the emissivity spectra of sample materials. b) Minimum emissivity (ε_{\min}) for TES channels estimated from the minimum-maximum emissivity difference (MMD) in the MERSI-LL FY-3E normalized emissivity method (NEM) module.

Fig. S4. a) Root Mean Square Error (RMSE) of Estimated Broadband Emissivity (BBE) using linear regression for each sensor-platform. b) Estimated BBE in this study comparing to previous study [1].

Fig. S5. Spatial patterns of land surface temperature (LST) estimated by (a) ABI GOES-16, and (b) MERSI-LL FY-3E, and MERSI-LL FY-3E channel emissivities (c-e) estimated in this study.

TABLE SI. Root Mean Square Error (RMSE, unit: Kelvin) and coefficients of estimated MERSI-LL FY-3E ground leaving equivalent brightness temperature (BT(Tg,i)) using the EMC/WVD method (equation 3 in the main text) at different VZAs and different bands.

TABLE SII. Simulated water vapor scaling (WVS) coefficients (a_i) for MERSI-LL FY-3E channels.

TABLE SIII. A list of 46 observation sites used for validating satellite-based land surface temperature in this study.

Reference for Supplementary Material

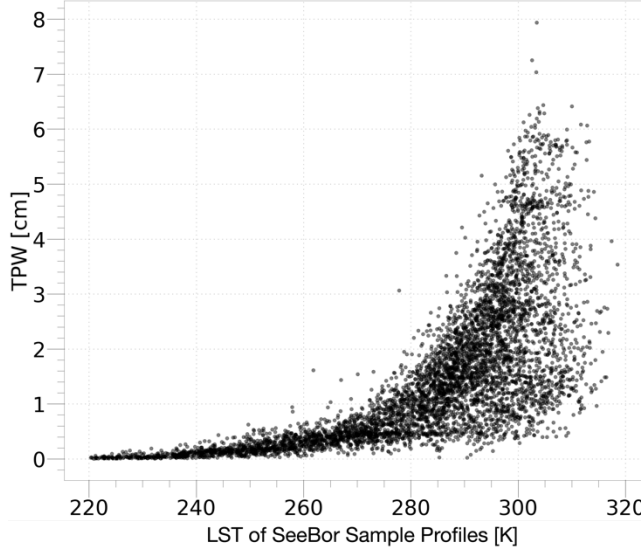


Fig. S1. Total Precipitable Water (TPW) and simulated land surface temperature (LST) for the SeeBor profile used in this study.

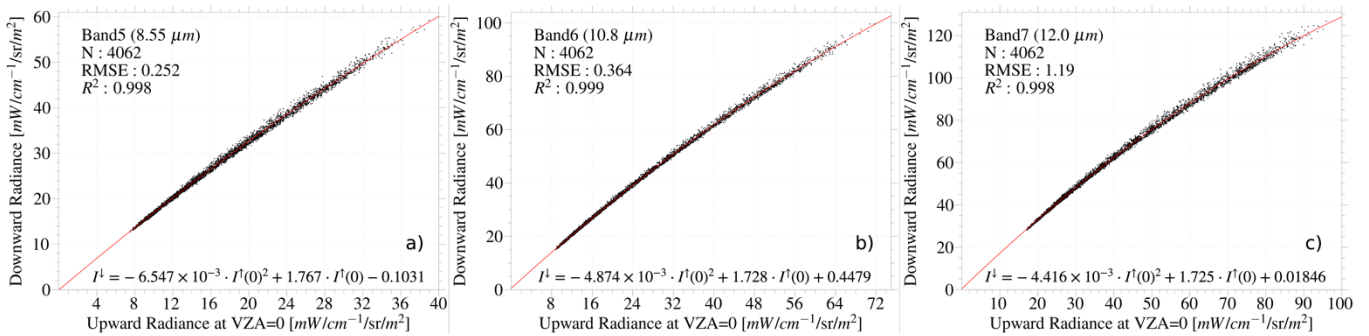


Fig. S2. Atmospheric downward radiance estimated from the atmospheric upward radiance of (a) band 5, (b) band 6, and (c) band 7 of the MERSI-LL FY-3E. Black dots represent simulated downwelling radiance values obtained using the nadir upwelling radiance. The red line represents the fitted curve.

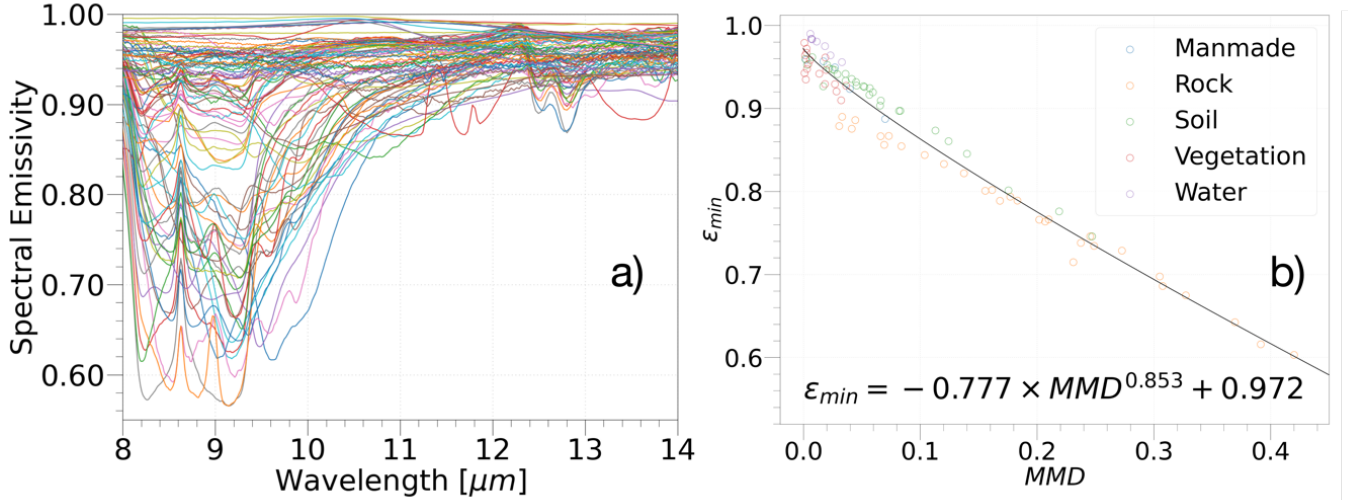


Fig. S3. a) Emissivity spectra of sample materials used for training the normalized emissivity method (NEM) module. Lines represent the emissivity spectra of sample materials. b) Minimum emissivity (ϵ_{min}) for TES channels estimated from the minimum-maximum emissivity difference (MMD) in the MERSI-LL FY-3E normalized emissivity method (NEM) module. Colored dots represent the minimum emissivity and MMD values for sample materials in the database. The black solid line represents the fitted line, with the ϵ_{min} using MMD as a variable.

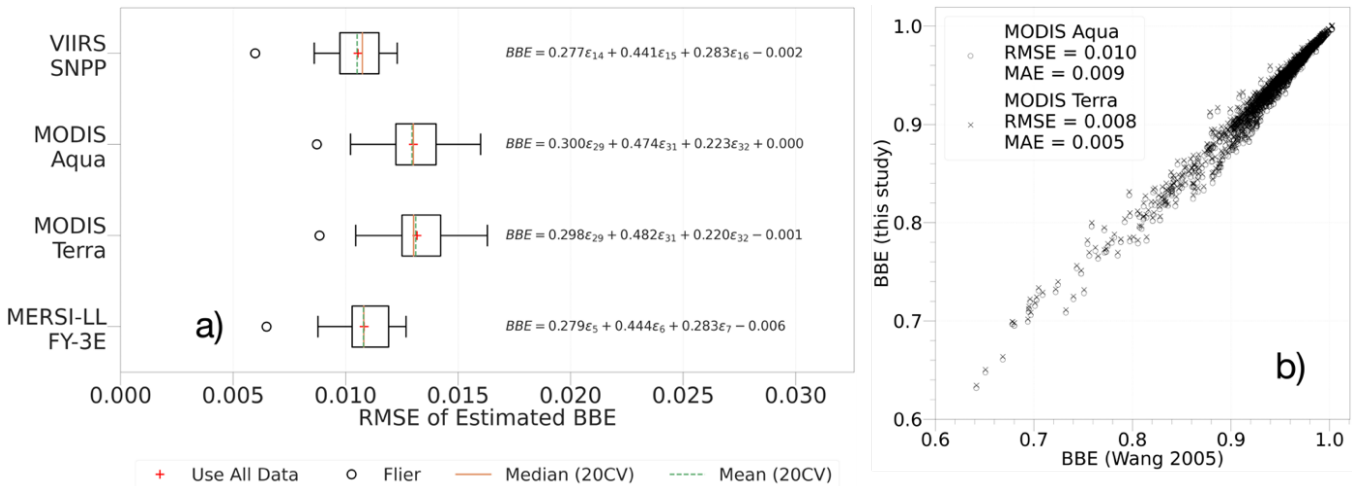


Fig. S4. a) Root Mean Square Error (RMSE) of Estimated Broadband Emissivity (BBE) using linear regression for each sensor-platform. The box plot represents the group RMSE of the estimated BBE in a 20-fold cross-validation. Red cross markers indicate training using all emissivity spectra and validation with the same data. Orange lines represent the median RMSE in the cross-validation groups, while green lines represent the average RMSE. b) Estimated BBE in this study comparing to previous study [1].

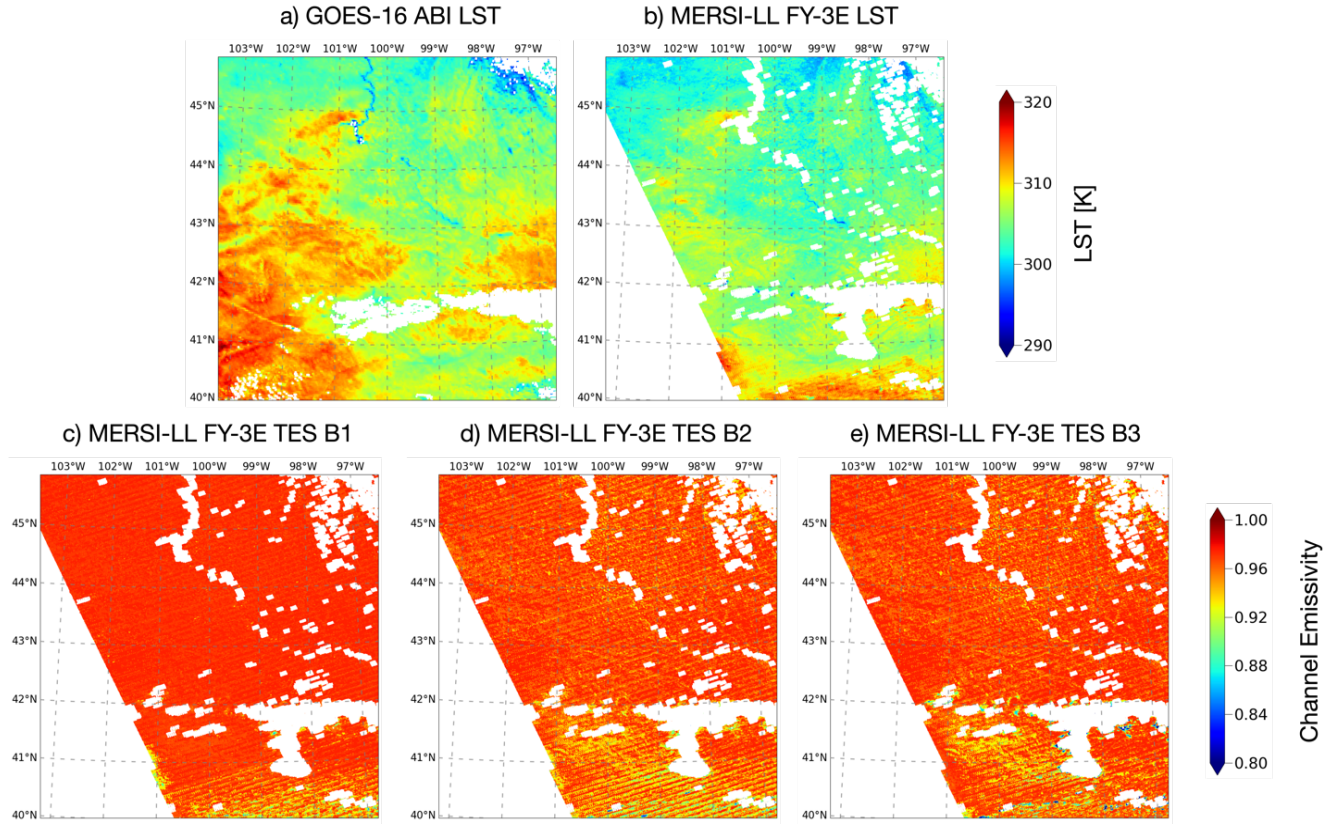


Fig. S5. Spatial patterns of land surface temperature (LST) estimated by (a) ABI GOES-16, and (b) MERSI-LL FY-3E, and MERSI-LL FY-3E channel emissivities (c-e) estimated in this study. The observation time is 16:15 on June 16 (local time), 2022 for ROI2.

TABLE SI

ROOT MEAN SQUARE ERROR (RMSE, UNIT: KELVIN) AND COEFFICIENTS OF ESTIMATED MERSI-LL FY-3E GROUND LEAVING EQUIVALENT BRIGHTNESS TEMPERATURE ($BT(TG,i)$) USING THE EMC/WVD METHOD (EQUATION 3 IN THE MAIN TEXT) AT DIFFERENT VZAS AND DIFFERENT BANDS. HERE, $p_{i,j}$, $q_{i,j}$, AND $r_{i,j}$ REPRESENT THE SIMULATED COEFFICIENTS.

VZA	Band	RMSE	$p_{i,0}$	$q_{i,0}$	$r_{i,0}$	$p_{i,5}$	$q_{i,5}$	$r_{i,5}$	$p_{i,6}$	$q_{i,6}$	$r_{i,6}$	$p_{i,7}$	$q_{i,7}$	$r_{i,7}$
0.00	5	0.191	-2.3439	0.3153	2.5702	-1.8741	0.1874	-0.2274	2.1857	-0.9583	0.8351	-0.3080	2.1821	-0.8773
	6	0.164	1.2136	0.3806	-0.1941	-0.1882	1.0315	0.3039	0.3299	-0.6363	0.0278	0.3925	0.2731	-0.6633
	7	0.185	-1.5724	-0.0052	-0.0027	0.0131	-1.3917	0.0386	-0.0983	0.0647	-1.2246	0.0293	-0.0934	0.0684
36.87	5	0.229	-2.4264	0.1893	2.5817	-1.7592	0.1864	-0.2671	2.2809	-1.0139	0.8360	-0.3372	2.2700	-0.9363
	6	0.210	1.9004	0.3824	-0.0756	-0.3110	1.4968	0.3327	0.3630	-0.6996	0.5941	0.3988	0.3259	-0.7242
	7	0.226	-2.2318	0.0174	-0.0365	0.0267	-2.0435	0.0529	-0.1203	0.0747	-1.8709	0.0463	-0.1177	0.0780
48.19	5	0.273	-2.3752	0.0835	2.6004	-1.6721	0.2325	-0.3029	2.3575	-1.0549	0.8814	-0.3649	2.3424	-0.9812
	6	0.260	2.5080	0.3939	0.0239	-0.4240	1.9392	0.3603	0.3973	-0.7628	1.1149	0.4120	0.3730	-0.7862
	7	0.274	-2.9792	0.0394	-0.0697	0.0406	-2.7835	0.0689	-0.1437	0.0849	-2.6096	0.0639	-0.1427	0.0881
55.15	5	0.322	-2.2605	-0.0036	2.6211	-1.6061	0.3006	-0.3345	2.4199	-1.0861	0.9482	-0.3899	2.4023	-1.0164
	6	0.314	3.0907	0.4072	0.1118	-0.5270	2.3999	0.3840	0.4346	-0.8250	1.6362	0.4261	0.4188	-0.8477
	7	0.326	-3.8177	0.0619	-0.1027	0.0543	-3.6161	0.0868	-0.1688	0.0952	-3.4426	0.0829	-0.1688	0.0983
60.00	5	0.376	-2.1206	-0.0752	2.6412	-1.5552	0.3748	-0.3618	2.4709	-1.1103	1.0217	-0.4121	2.4521	-1.0445
	6	0.372	3.7251	0.4178	0.1941	-0.6220	2.9410	0.4018	0.4768	-0.8867	2.2231	0.4373	0.4668	-0.9086
	7	0.382	-4.7586	0.0857	-0.1363	0.0676	-4.5517	0.1070	-0.1959	0.1055	-4.3787	0.1038	-0.1966	0.1087
63.61	5	0.435	-1.9857	-0.1339	2.6590	-1.5149	0.4375	-0.3851	2.5124	-1.1288	1.0844	-0.4312	2.4930	-1.0667
	6	0.434	4.4572	0.4241	0.2746	-0.7112	3.5987	0.4136	0.5247	-0.9484	2.9150	0.4444	0.5185	-0.9695
	7	0.443	-5.8069	0.1113	-0.1712	0.0808	-5.5945	0.1297	-0.2252	0.1161	-5.4218	0.1269	-0.2264	0.1193
66.42	5	0.606	-1.7373	-0.2222	2.6032	-1.3719	0.5262	-0.4268	2.4868	-1.0619	1.1615	-0.4668	2.4676	-1.0062
	6	0.607	5.3635	0.3849	0.4797	-0.8805	4.3609	0.3833	0.6829	-1.0790	3.7120	0.4094	0.6791	-1.0980
	7	0.613	-6.8123	0.1506	-0.2225	0.0968	-6.5754	0.1645	-0.2680	0.1278	-6.4017	0.1620	-0.2693	0.1309

TABLE SII

SIMULATED WATER VAPOR SCALING (WVS) COEFFICIENTS (a_i) FOR MERSI-LL FY-3E CHANNELS. THE ROOT MEAN SQUARE ERROR (RMSE: UNITLESS) FOR WAS CALCULATED USING A WVS FACTOR (γ) OF 0.9, γ_1 OF 1.0, γ_2 OF 0.7 (EQUATION 4 IN THE MAIN TEXT).

Band No. (i)	Band5	Band6	Band7
Coefficient (a_i)	1.453	1.841	1.783
RMSE of γ	2.752×10^{-3}	1.324×10^{-3}	1.614×10^{-3}

TABLE SIII

A LIST OF 46 OBSERVATION SITES USED FOR VALIDATING SATELLITE-BASED LAND SURFACE TEMPERATURE IN THIS STUDY.

ID	Network	Latitude	Longitude	Altitude	LC (Land cover category)	Reference
US-ARM	AmeriFlux	36.6058 °N	97.4888 °W	314 m	low_vegetation	[2]
US-Bi1	AmeriFlux	38.0992 °N	121.4993 °W	-2.7 m	low_vegetation	[3]
US-Bi2	AmeriFlux	38.1091 °N	121.5351 °W	-5 m	low_vegetation	[4]
US-Prr	AmeriFlux	65.1237 °N	147.4876 °W	210 m	tree	[5]
US-RGB	AmeriFlux	39.5782 °N	121.8579 °W	33 m	low_vegetation	[6]
US-Rms	AmeriFlux	43.0645 °N	116.7486 °W	2111 m	low_vegetation	[7]
US-Rpf	AmeriFlux	65.1198 °N	147.4290 °W	497 m	tree	[8]
US-Uaf	AmeriFlux	64.8663 °N	147.8555 °W	155 m	tree	[9]
US-xAB	AmeriFlux	45.7624 °N	122.3303 °W	363 m	tree	[10]
US-xAE	AmeriFlux	35.4106 °N	99.0588 °W	516 m	low_vegetation	[11]
US-xBN	AmeriFlux	65.1540 °N	147.5026 °W	263 m	tree	[12]
US-xDJ	AmeriFlux	63.8811 °N	145.7514 °W	529 m	tree	[13]
US-xKZ	AmeriFlux	39.1008 °N	96.5631 °W	381 m	low_vegetation	[14]
US-xMB	AmeriFlux	38.2483 °N	109.3883 °W	1767 m	low_vegetation	[15]
US-xNG	AmeriFlux	46.7697 °N	100.9154 °W	578 m	low_vegetation	[16]
US-xNQ	AmeriFlux	40.1776 °N	112.4524 °W	1685 m	low_vegetation	[17]
US-xRN	AmeriFlux	35.9641 °N	84.2826 °W	334 m	tree	[18]
US-xSE	AmeriFlux	38.8901 °N	76.5600 °W	15 m	tree	[19]
US-xST	AmeriFlux	45.5089 °N	89.5864 °W	481 m	tree	[20]
US-xTR	AmeriFlux	45.4937 °N	89.5857 °W	472 m	tree	[21]
US-xUK	AmeriFlux	39.0404 °N	95.1921 °W	335 m	tree	[22]
US-xUN	AmeriFlux	46.2339 °N	89.5373 °W	518 m	tree	[23]
US-xWD	AmeriFlux	47.1282 °N	99.2414 °W	579 m	low_vegetation	[24]
US-xWR	AmeriFlux	45.8205 °N	121.9519 °W	407 m	tree	[25]
BE-Bra	ICOS	51.3076 °N	4.5198 °E	16 m	tree	[26]
BE-Lon	ICOS	50.5516 °N	4.7462 °E	170 m	low_vegetation	[27]
BE-Maa	ICOS	50.9799 °N	5.6319 °E	87 m	tree	[28]
CZ-Lnz	ICOS	48.6816 °N	16.9463 °E	150 m	tree	[29]
DE-Geb	ICOS	51.0997 °N	10.9146 °E	161.5 m	low_vegetation	[30]

DE-HoH	ICOS	52.0866 °N	11.2224 °E	193 m	tree	[31]
DE-Tha	ICOS	50.9626 °N	13.5652 °E	380 m	tree	[32]
DK-Sor	ICOS	55.4859 °N	11.6446 °E	40 m	tree	[33]
FI-Hyy	ICOS	61.8474 °N	24.2948 °E	181 m	tree	[34]
FR-Fon	ICOS	48.4764 °N	2.7801 °E	103 m	tree	[35]
FR-Hes	ICOS	48.6741 °N	7.0647 °E	310 m	tree	[36]
FR-Pue	ICOS	43.7413 °N	3.5957 °E	271 m	tree	[37]
IT-Cp2	ICOS	41.7043 °N	12.3573 °E	19 m	tree	[38]
IT-Ren	ICOS	46.5869 °N	11.4337 °E	1735.6 m	tree	[39]
IT-SR2	ICOS	43.7320 °N	10.2909 °E	4 m	tree	[40]
SE-Htm	ICOS	56.0976 °N	13.4190 °E	115 m	tree	[41]
SE-Nor	ICOS	60.0865 °N	17.4795 °E	45 m	tree	[42]
SE-Svb	ICOS	64.2561 °N	19.7745 °E	267 m	tree	[43]
bon	SURFRAD	40.0500 °N	88.3700 °W	213 m	low_vegetation	[44]
dra	SURFRAD	36.6240 °N	116.0190 °W	1007 m	solid (barren)	[44]
fpk	SURFRAD	48.3100 °N	105.1000 °W	634 m	low_vegetation	[44]
sxf	SURFRAD	43.7300 °N	96.6200 °W	473 m	low_vegetation	[44]

References for Supplementary Material

- [1] K. Wang et al., "Estimation of Surface Long Wave Radiation and Broadband Emissivity Using Moderate Resolution Imaging Spectroradiometer (MODIS) Land Surface Temperature/Emissivity Products," *Journal of Geophysical Research: Atmospheres*, vol. 110, no. D11, 2005. [Online]. Available: <https://doi.org/10.1029/2004JD005566>.
- [2] S. Biraud, M. Fischer, S. Chan, and M. Torn, "AmeriFlux BASE US-ARM ARM Southern Great Plains site- Lamont, Ver. 12-5," AmeriFlux AMP, 2023. [Dataset]. Available: <https://doi.org/10.17190/AMF/1246027>.
- [3] C. Rey-Sanchez et al., "AmeriFlux BASE US-Bi1 Bouldin Island Alfalfa, Ver. 9-5," AmeriFlux AMP, 2023. [Dataset]. Available: <https://doi.org/10.17190/AMF/1480317>.
- [4] C. Rey-Sanchez, C. T. Wang, D. Szutu, K. Hemes, J. Verfaillie, and D. Baldocchi, "AmeriFlux BASE US-Bi2 Bouldin Island corn, Ver. 14-5," AmeriFlux AMP, 2023. [Dataset]. Available: <https://doi.org/10.17190/AMF/1419513>.
- [5] T. Nakai et al., "Characteristics of evapotranspiration from a permafrost black spruce forest in interior Alaska," *Polar Science*, vol. 7, pp. 136-148, 2013. [Online]. Available: <https://doi.org/10.1016/j.polar.2013.03.003>.
- [6] M. Schuppenhauer and S. C. Biraud, "AmeriFlux BASE US-RGB Butte County Rice Farm, Ver. 3-5," AmeriFlux AMP, 2023. [Dataset]. Available: <https://doi.org/10.17190/AMF/1870591>.
- [7] G. Flerchinger, "AmeriFlux BASE US-Rms RCEW Mountain Big Sagebrush, Ver. 5-5," AmeriFlux AMP, 2023. [Dataset]. Available: <https://doi.org/10.17190/AMF/1375202>.
- [8] M. Ueyama, H. Iwata, and Y. Harazono, "AmeriFlux BASE US-Rpf Poker Flat Research Range: Succession from fire scar to deciduous forest, Ver. 9-5," AmeriFlux AMP, 2023. [Dataset]. Available: <https://doi.org/10.17190/AMF/1579540>.
- [9] M. Ueyama, H. Iwata, and Y. Harazono, "AmeriFlux BASE US-Uaf University of Alaska, Fairbanks, Ver. 11-5," AmeriFlux AMP, 2023. [Dataset]. Available: <https://doi.org/10.17190/AMF/1480322>.
- [10] NEON (National Ecological Observatory Network), "AmeriFlux BASE US-xAB NEON Abby Road (ABBY), Ver. 7-5," AmeriFlux AMP, 2023. [Dataset]. Available: <https://doi.org/10.17190/AMF/1617726>.
- [11] NEON (National Ecological Observatory Network), "AmeriFlux BASE US-xAE NEON Klemme Range Research Station (OAES), Ver. 6-5," AmeriFlux AMP, 2023. [Dataset]. Available: <https://doi.org/10.17190/AMF/1671891>.
- [12] NEON (National Ecological Observatory Network), "AmeriFlux BASE US-xBN NEON Caribou Creek - Poker Flats Watershed (BONA), Ver. 7-5," AmeriFlux AMP, 2023. [Dataset]. Available: <https://doi.org/10.17190/AMF/1617727>.
- [13] NEON (National Ecological Observatory Network), "AmeriFlux BASE US-xDJ NEON Delta Junction (DEJU), Ver. 7-5," AmeriFlux AMP, 2023. [Dataset]. Available: <https://doi.org/10.17190/AMF/1634884>.
- [14] NEON (National Ecological Observatory Network), "AmeriFlux BASE US-xKZ NEON Konza Prairie Biological Station (KONZ), Ver. 8-5," AmeriFlux AMP, 2023. [Dataset]. Available: <https://doi.org/10.17190/AMF/1562392>.
- [15] NEON (National Ecological Observatory Network), "AmeriFlux BASE US-xMB NEON Moab (MOAB), Ver. 6-5," AmeriFlux AMP, 2023. [Dataset]. Available: <https://doi.org/10.17190/AMF/1671896>.
- [16] NEON (National Ecological Observatory Network), "AmeriFlux BASE US-xNG NEON Northern Great Plains Research Laboratory (NOGP), Ver. 7-5," AmeriFlux AMP, 2023. [Dataset]. Available: <https://doi.org/10.17190/AMF/1617732>.
- [17] NEON (National Ecological Observatory Network), "AmeriFlux BASE US-xNQ NEON Onaqui-Ault (ONAQ), Ver. 7-5," AmeriFlux AMP, 2023. [Dataset]. Available: <https://doi.org/10.17190/AMF/1617733>.
- [18] NEON (National Ecological Observatory Network), "AmeriFlux BASE US-xRN NEON Oak Ridge National Lab (ORNL), Ver. 5-5," AmeriFlux AMP, 2023. [Dataset]. Available: <https://doi.org/10.17190/AMF/1773400>.
- [19] NEON (National Ecological Observatory Network), "AmeriFlux BASE US-xSE NEON Smithsonian Environmental Research Center (SERC), Ver. 7-5," AmeriFlux AMP, 2023. [Dataset]. Available: <https://doi.org/10.17190/AMF/1617734>.
- [20] NEON (National Ecological Observatory Network), "AmeriFlux BASE US-xST NEON Steigerwaldt Land Services (STEI), Ver. 7-5," AmeriFlux AMP, 2023. [Dataset]. Available: <https://doi.org/10.17190/AMF/1617737>.
- [21] NEON (National Ecological Observatory Network), "AmeriFlux BASE US-xTR NEON Treehaven (TREE), Ver. 7-5," AmeriFlux AMP, 2023. [Dataset]. Available: <https://doi.org/10.17190/AMF/1634886>.
- [22] NEON (National Ecological Observatory Network), "AmeriFlux BASE US-xUK NEON The University of Kansas Field Station (UKFS), Ver. 7-5," AmeriFlux AMP, 2023. [Dataset]. Available: <https://doi.org/10.17190/AMF/1617740>.
- [23] NEON (National Ecological Observatory Network), "AmeriFlux BASE US-xUN NEON University of Notre Dame Environmental Research Center (UNDE), Ver. 7-5," AmeriFlux AMP, 2023. [Dataset]. Available: <https://doi.org/10.17190/AMF/1617741>.
- [24] NEON (National Ecological Observatory Network), "AmeriFlux BASE US-xWD NEON Woodworth (WOOD), Ver. 7-5," AmeriFlux AMP, 2023. [Dataset]. Available: <https://doi.org/10.17190/AMF/1579724>.
- [25] NEON (National Ecological Observatory Network), "AmeriFlux BASE US-xWR NEON Wind River Experimental Forest (WREF), Ver. 7-5," AmeriFlux AMP, 2023. [Dataset]. Available: <https://doi.org/10.17190/AMF/1617742>.

- [26] I. Janssens et al., "ETC L2 Meteo, Brasschaat, 2019-12-31–2022-12-31," ICOS RI, 2023. [Online]. Available: <https://hdl.handle.net/11676/DAPTxDX21Rm-AfFjXTJ8KD3y>.
- [27] B. Dumont et al., "ETC L2 Meteo, Lonzee, 2016-12-31–2022-12-31," ICOS RI, 2023. [Online]. Available: https://hdl.handle.net/11676/J1CfUMJsqJcP_gEUwgrRd1E6.
- [28] M. Roland et al., "ETC L2 Meteo, Maasmechelen, 2019-12-31–2022-12-31," ICOS RI, 2023. [Online]. Available: https://hdl.handle.net/11676/V1kAxU6_3ez5ykjNdNfluKT5.
- [29] N. Kowalska et al., "ETC L2 Meteo, Lanzhot, 2021-12-31–2022-12-31," ICOS RI, 2023. [Online]. Available: <https://hdl.handle.net/11676/BbWD7uf6KrOIV03JMaVy354Q>.
- [30] C. Brümmer, J. Delorme, and F. Schrader, "ETC L2 Meteo, Gebesee, 2019-12-31–2022-12-31," ICOS RI, 2023. [Online]. Available: <https://hdl.handle.net/11676/TZeFJMtfNUapv0D1kHLD9jf09>.
- [31] C. Rebmann et al., "ETC L2 Meteo, Hohes Holz, 2018-12-31–2022-12-31," ICOS RI, 2023. [Online]. Available: https://hdl.handle.net/11676/7mm_2Pj2nZTS17JBdLbkMaE7.
- [32] C. Bernhofer et al., "ETC L2 Meteo, Tharandt, 2019-12-31–2022-12-31," ICOS RI, 2023. [Online]. Available: <https://hdl.handle.net/11676/-5gGiobhYOiKZHEUE11wxvdW>.
- [33] A. Ibrom et al., "ETC L2 Meteo, Soroe, 2020-12-31–2022-12-31," ICOS RI, 2023. [Online]. Available: <https://hdl.handle.net/11676/7M6prRRYWwR4XlrTrYKrg-gI>.
- [34] I. Mammarella et al., "ETC L2 Meteo, Hyttiala, 2017-12-31–2022-12-31," ICOS RI, 2023. [Online]. Available: <https://hdl.handle.net/11676/kMpEN0Sz0xX6iagfzQJISgCn>.
- [35] D. Berveiller et al., "ETC L2 Meteo, Fontainebleau-Barbeau, 2018-12-31–2022-12-31," ICOS RI, 2023. [Online]. Available: https://hdl.handle.net/11676/2NssCcrzY_nglLsDjhMeyoW6.
- [36] M. Cuntz et al., "ETC L2 Meteo, Hesse, 2021-12-31–2022-12-31," ICOS RI, 2023. [Online]. Available: <https://hdl.handle.net/11676/Sc-Eml83LPq-m1uEPUv7OYru>.
- [37] J. Limousin, J. Kempf, and J. Ourcival, "ETC L2 Meteo, Puechabon, 2020-12-31–2022-12-31," ICOS RI, 2023. [Online]. Available: <https://hdl.handle.net/11676/jZakJsrC1V76xMFAr3jKvd0m>.
- [38] S. Fares et al., "ETC L2 Meteo, Castelporziano2, 2020-12-31–2022-12-31," ICOS RI, 2023. [Online]. Available: https://hdl.handle.net/11676/X_VOhZRs43iPDK50G3-qp0qo.
- [39] L. Montagnani et al., "ETC L2 Meteo, Renon, 2020-12-31–2022-12-31," ICOS RI, 2023. [Online]. Available: <https://hdl.handle.net/11676/2wlkuUr8h10l0EyflIdQVATgj>.
- [40] N. Arriga et al., "ETC L2 Meteo, San Rossore 2, 2018-12-31–2022-12-31," ICOS RI, 2023. [Online]. Available: <https://hdl.handle.net/11676/sNAafBpVZokhD8rG4VYVdA2a>.
- [41] M. Heliasz et al., "ETC L2 Meteo, Hyltemossa, 2017-12-31–2022-12-31," ICOS RI, 2023. [Online]. Available: <https://hdl.handle.net/11676/zhcocG7rA9oJAJK89hyjCyrD>.
- [42] M. Mölder et al., "ETC L2 Meteo, Norunda, 2017-12-31–2022-12-31," ICOS RI, 2023. [Online]. Available: <https://hdl.handle.net/11676/7vZZUhXD-dLedudgSseUk5Ys>.
- [43] M. Peichl et al., "ETC L2 Meteo, Svartberget, 2018-12-31–2022-12-31," ICOS RI, 2023. [Online]. Available: <https://hdl.handle.net/11676/qPUER-xPefUYiR2NP3LJwK0W>.
- [44] J.A. Augustine, J.J. DeLuisi, and C.N. Long, "SURFRAD—A National Surface Radiation Budget Network for Atmospheric Research," Bull. Amer. Meteor. Soc., vol. 81, pp. 2341–2357, 2000. [Online]. Available: [https://doi.org/10.1175/1520-0477\(2000\)081<2341:SANSRB>2.3.CO;2](https://doi.org/10.1175/1520-0477(2000)081<2341:SANSRB>2.3.CO;2).